ACS APPLIED MATERIALS & INTERFACES

Research Article

www.acsami.org

Triboelectric Nanogenerators as a Self-Powered 3D Acceleration Sensor

Yao Kun Pang,[†] Xiao Hui Li,[†] Meng Xiao Chen,[†] Chang Bao Han,[†] Chi Zhang,*[,†] and Zhong Lin Wang*[,†,‡]

[†]Beijing Institute of Nanoenergy and Nanosystems, Chinese Academy of Sciences, Beijing, 100083, China

[‡]School of Material Science and Engineering, Georgia Institute of Technology, Atlanta, Georgia 30332, United States

Supporting Information

ABSTRACT: A novel self-powered acceleration sensor based on triboelectric nanogenerator is proposed, which consists of an outer transparent shell and an inner mass-spring-damper mechanical system. The PTFE films on the mass surfaces can slide between two aluminum electrodes on an inner wall owing to the acceleration in the axis direction. On the basis of the coupling of triboelectric and electrostatic effects, the potential difference between the two aluminum electrodes is generated in proportion to the mass displacement, which can be used to characterize the acceleration in the axis direction with a detection range from about 13.0 to 40.0 m/s^2 at a sensitivity of 0.289 V·s^2/m. With the integration of acceleration sensors in three axes, a self-powered 3D acceleration sensor is developed for vector acceleration measurement in any direction. The self-powered 3D acceleration sensor has excellent performance in the stability test, and the output voltages have a little decrease of ∼6% after 4000 cycles. Moreover, the self-powered acceleration sensor can be used to measure high collision acceleration, which has potential practicability in automobile security systems.

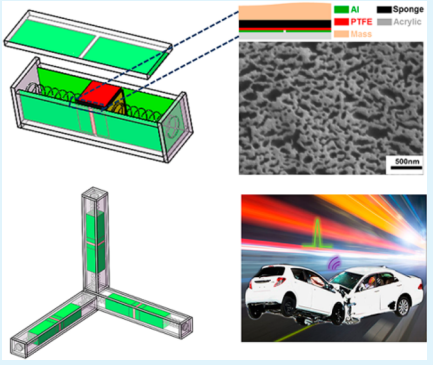

KEYWORDS: *triboelectric nanogenerator, self-powered sensor, acceleration sensor, 3D, automobile collision*

INTRODUCTION

An acceleration sensor is a device that can measure accelerating force, which plays an important role in many fields, such as satellites, biomedical devices, large mechanical structure testing, airbags, and earthquake monitoring.[1,2] According to the different physical principles, acceleration sensors can be broadly classified into capacitive,[3,4] piezoresistive,[5] and piezoelectric[6−8] types, in which the capacitive and piezoresistive sensors require external power, which may limit their wide application. The piezoelectric sensor is self-powered, but the output electrical signal is very small and may be influenced by the environmental noise. It is necessary, therefore, to fabricate an acceleration sensor, which does not need an external power source and has large output signal. One of the practicable approaches is to convert the ambient environment energy (such as solar energy, wind energy, geothermal energy) into electrical energy to drive the sensor,[9−12] while the other important approach is that the sensor can actively generate an electric signal itself as a response to the acceleration.[13]

Recently, the triboelectric nanogenerator (TENG) based on triboelectric and electrostatic induction effects has been successfully invented to harvest mechanical energy.[14−16] To now, owing to the outstanding performance and high output voltage, the TENG has been extensively used to drive or control microelectronic devices[17−20] and act as self-powered sensors, such as motion tracking,[21] pressure,[22] touch,[23−25] acoustic,[26,27] and vibration sensors,[28−30] and it also could be used to act as a self-powered acceleration sensor.

In this paper, we demonstrated a novel self-powered 3D acceleration sensor based on three independent TENGs, which were perpendicular in the three directions and composed of an outer transparent shell and an inner mass−spring−damper mechanical system. Owing to the linearly proportional relationship between the acceleration and the output voltage, the sensor can be used to measure acceleration with great detection range and sensitivity. More importantly, the 3D acceleration sensor can be used to measure vector acceleration in any direction and the components of the vector acceleration in the three axes can be characterized by the three output voltages, respectively and independently. Furthermore, high speed car collision acceleration was simulated and successfully detected by the self-powered 3D acceleration sensor, which has a potential practicability in automobile security systems.

RESULT AND DISCUSSION

Figure 1a schematically shows the basic structure of the 1D self-powered acceleration sensor based on a single TENG, which consists of an outer transparent shell and an inner mass−spring−damper mechanical system. In the fabrication process,

Received: May 24, 2015
Accepted: August 11, 2015

DOI: 10.1021/acsami.5b04516
ACS Appl. Mater. Interfaces XXXX, XXX, XXX−XXX

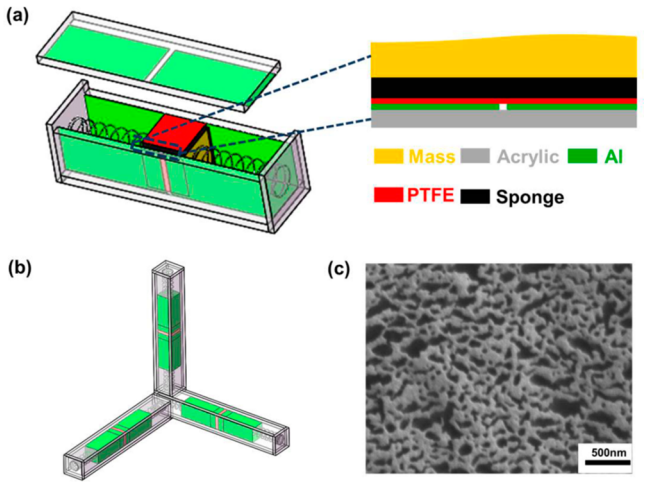

Figure 1. Basic structure of the self-powered 3D acceleration sensor based on TENGs. (a) Schematic illustrations of 1D acceleration sensor based on single TENG. (b) Schematic diagram showing the structural design of the device composed of three TENGs. (c) SEM image of the PTFE surface with etched nanostructure.

the outer transparent shell was composed of acrylic sheets, which were accurately cut by a laser cutter and have the distinct advantages of low weight, low cost, and great machinability. The cubical inertial mass is made of steel, with the side length of 18 mm and the weight of 28.45 g. As the fixed triboelectric layers and electrodes, two pieces of Al films (18 mm × 40 mm) were pasted on the internal surface of the acrylic sheets, leaving an interval less than 1 mm between them. The polytetrafluoroethylene (PTFE) film was purposely chosen as the freestanding triboelectric layer, which was cut into 18 mm × 18 mm and adhered on the surface of the inertial mass. In order to increase the effective contact surface area and the surface roughness and effectively improve the output signal of the TENG, nanostructures (Figure 1c) were processed on the PTFE surface by the inductive coupled plasma (ICP). A piece of sponge was sandwiched between the mass and the PTFE film as a buffer, which can maintain intimate contact between the Al and PTFE films for electrification and improve the stability of the sensor. Two springs with spring coefficients of 42.96 N/m and lengths of 50 mm were fixed on two opposite sides of the mass, which can restrain the mass at the initial position without external acceleration. Figure 1b shows the structural design of the 3D acceleration sensor, which is composed of three perpendicular 1D acceleration sensors for measuring the acceleration with respect to the *X*, *Y*, and *Z* axes, respectively.

Figure 2 schematically displays the working principle of the acceleration sensor. As shown in Figure 2a, when the PTFE film is intimately contacted with the two Al electrodes in the middle position, owing to the different triboelectric polarity of the PTFE and Al, the electrons will transfer from the Al electrodes to the PTFE film, rendering the PTFE film with negative charges in the saturated state and the two pieces of Al film electrodes with equal positive charges in average, which will not generate potential difference between them due to electrostatic equilibrium. The charges on the PTFE surface cannot be conducted away or neutralized in the measurement process. When the acceleration sensor is subject to a certain external acceleration in the left-hand direction, the left-hand side spring will be stretched while the right-hand side spring will be compressed. Meanwhile, the PTFE film will slide against with the Al electrodes (Figure 2b) owing to the inertia force. On the left-hand Al electrode, part of positive charges will lose the constraints of the negative charges on the PTFE surface and be evenly distributed on the part of left-hand Al electrode, which is not contacted with the PTFE film. While on the right-hand Al electrode, all of the positive charges will be evenly distributed on the part of right-hand Al electrode, which is

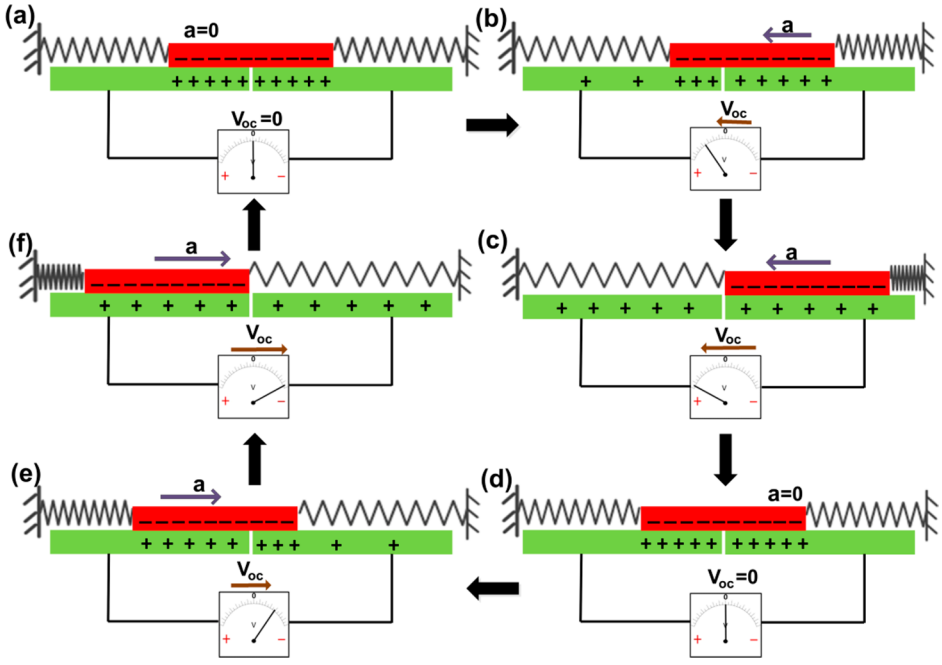

Figure 2. Working principle of the acceleration sensor. (a) Original state with the PTFE in the middle position. (b) PTFE film sliding to the right and separating with the left electrode. (c) PTFE film slides out of the left-hand electrode. (d) Returning to the original position. (e, f) PTFE film sliding in the opposite direction.

DOI: 10.1021/acsami.5b04516
ACS Appl. Mater. Interfaces XXXX, XXX, XXX−XXX

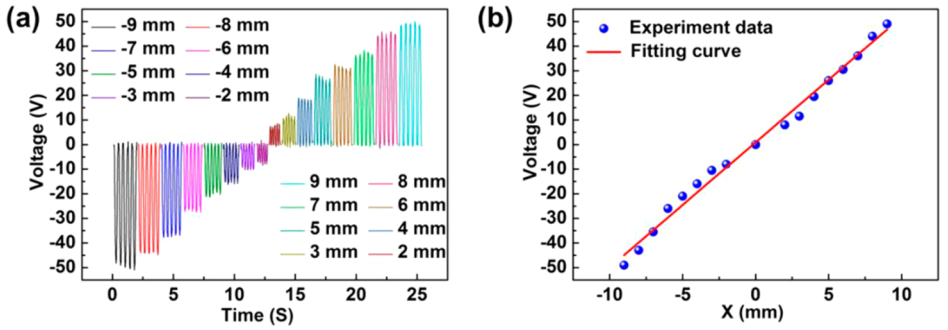

Figure 3. Relationship between the output voltages and the sliding displacements of the PTFE film. (a) Output voltage of the acceleration sensor when the PTFE slides from −9 to 9 mm. (b) Relationship between the output voltage and the sliding displacement, showing that they have a good linear relationship.

contacted with the PTFE film. There will be a positive potential difference between the two electrodes. With the increasing acceleration, the mass will slide to the right-hand side until the PTFE film slides out of the left-hand electrode (Figure 2c), and all of the positive charges on the left-hand Al electrode will lose the constraints and evenly distributed on the total left-hand Al electrode surface. While on the part of right-hand Al electrode, which is contacted with the whole PTFE film, all of the positive charges will be evenly distributed.The potential difference will reach the maximal value. After that, if the acceleration stops, the mass with the PTFE films will come back to its original position due to the elasticity of the springs (Figure 2d) and the potential difference will decrease to zero. The similar distribution of charges on the Al electrodes and potential difference with the reverse polarity are shown in Figures 2e and f. Therefore, the single TENG as a 1D self-powered acceleration sensor can characterize the acceleration vector in the axial direction.

The relationship between the output voltages and the sliding displacements of the PTFE film was systematically studied. As shown in Figure S1 (Supporting Information), the Al electrodes were fixed on the acrylic sheet and the inertial mass was fixed on the linear motor. The velocity and the acceleration of the linear motor are in oscillation and the frequency is fixed. At the original state, the inertial mass is in the middle of the Al electrodes. With the oscillation of the linear motor, the PTFE film slides against the Al electrodes and the sliding distance of the PTFE film from the original position can be precisely controlled by the linear motor. Figure 3a shows the output voltages of the acceleration sensor with the PTFE film sliding range from −9 to 9 mm. The output voltage increases with the sliding displacement, in which the polarity is determined by the sliding direction. As shown in Figure 3b, it is distinctly demonstrated that the output voltage has a good linear relationship with the sliding displacement.

The relationship between the acceleration and the output voltage is analyzed in Figure S2 (Supporting Information), in which the charges distribution in the surfaces is shown in detail. The TENG can be approximately considered as a capacitance. Thus, the output voltage can be described as follows:

$$V_{oc} = \frac{QL_x}{LC_0} \tag{1}$$

where V_{oc} is the open-circuit voltage of the sensor, Q is the total charges on the surface of the PTFE film, C_0 is the capacitance of the two Al electrodes, L is the length of the PTFE film, and L_x is the sliding distance of the PTFE film from the original position. The derivation of eq 1 is detailed in the Supporting Information. Considering to the complex structure and force conditions of the acceleration sensor in measurement, N_1, N_2, N_3, and N_4 are used to represent the pressure for each frictional surface, respectively, and μ to represent the identical friction coefficient owing to the same materials. The elastic force is represented as $2kL_x$ for the mass is forced by two identical springs. Therefore, the mechanics formula can be described as follows:

$$F = 2kL_x - \mu(N_1 + N_2 + N_3 + N_4) = ma \tag{2}$$

where k is spring coefficient, m is the weight of the mass, and a is the acceleration along movement direction of the inertial mass. With the above mechanics formula and the eq 1, the acceleration can be described as follows:

$$a = \frac{2kLC_0V_{oc}}{Qm} - \frac{\mu(N_1 + N_2 + N_3 + N_4)}{m} \tag{3}$$

Therefore, it is obviously demonstrated that the acceleration has a linear relationship with the output voltage. In the experiment, the sensitivity of the sensor can be calculated by $\Delta V/\Delta a$. According to eq 3, the sensitivity of the sensor can be described as follows:

$$S = \frac{Qm}{2kLC_0} \tag{4}$$

in which the sensitivity of the sensor is depended on the charges on the frictional surface, the inertial mass, the friction coefficient, the length of the PTFE film and the capacitance of the two Al electrodes.

Figure 4 shows the performance of the acceleration sensor. In the measurement process, the periodical positive and negative accelerations with the same magnitude were applied to the sensor for periodic reciprocating motion by a linear motor. The output voltages of the sensor at several specific accelerations are shown in Figures 4a−e. It can be seen clearly that all of the output voltage signals are uniform and stable. The relationship between the output voltage and the acceleration along the $+X$ direction and $-X$ are plotted in Figure 4f and Figure S3 (Supporting Information), which can be linearly fitted with the correlation coefficient of 0.990. Also, the sensor has a high sensitivity of 0.289 V·s^2/m, which is important to the applications of acceleration sensor. Figure 4g is the stability test of the acceleration sensor with periodical positive and negative acceleration of ±17 m/s^2 for 4000 cycles. The voltage was measured after every 500 cycles, during which 120 cycles were recorded. After 4000 cycles, the output voltages only show a

DOI: 10.1021/acsami.5b04516
ACS Appl. Mater. Interfaces XXXX, XXX, XXX−XXX

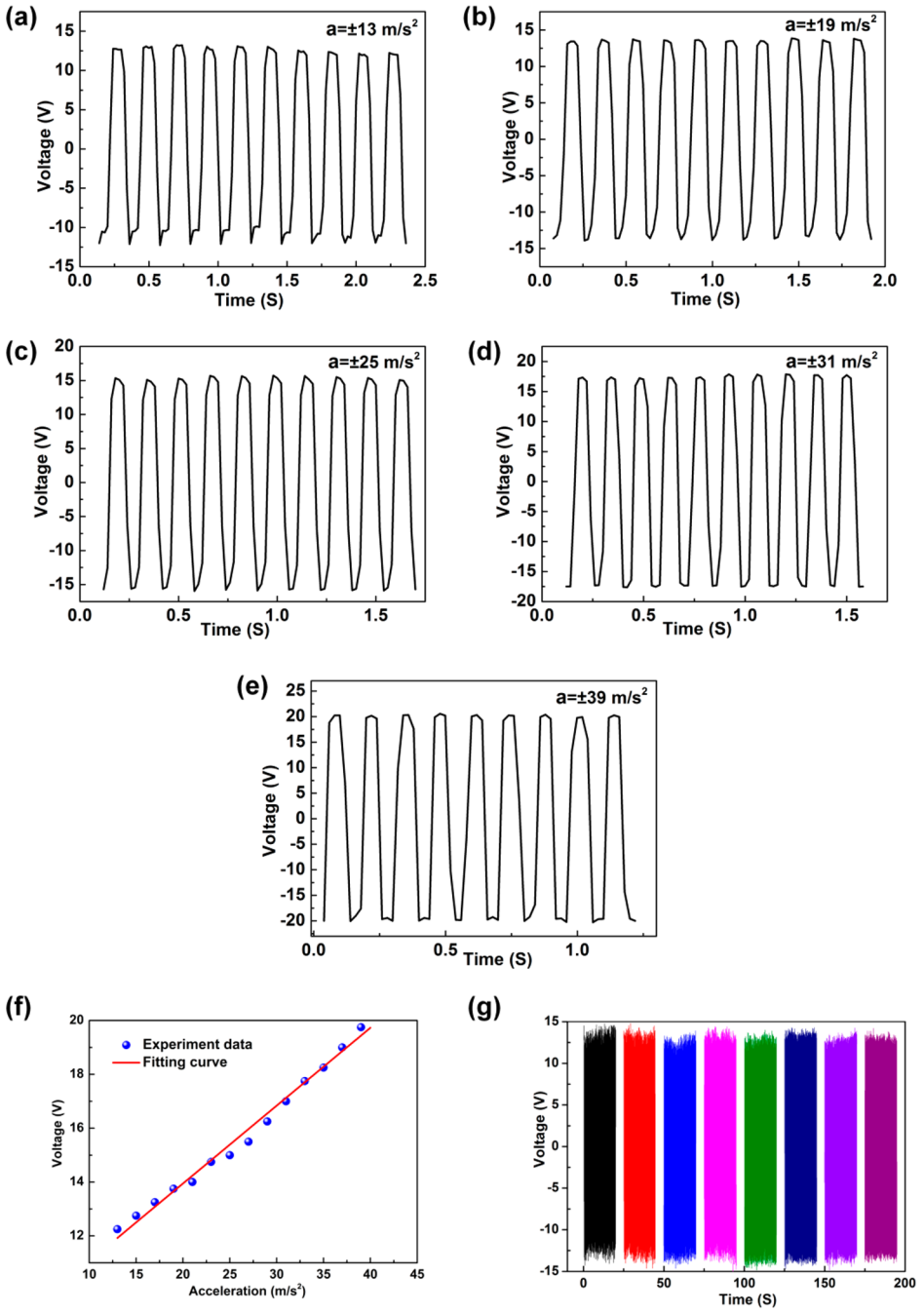

Figure 4. Performances of the acceleration sensor based on TENG. (a–e) Output voltages of the sensor at several specific accelerations. (f) The relationship between the positive peak value of output voltages and the corresponding accelerations. (g) The stability experiment of the acceleration sensor with periodical positive and negative accelerations (±17 m/s^2) for 4000 cycles.

little decay of ∼6%, which demonstrates that the sensor has an excellent stability. Therefore, the output voltage can successfully characterize the external acceleration.

On the basis of three perpendicular TENGs, the 3D acceleration sensor was developed and the characteristic calibrations in three axes are shown in Figure 5. When the 3D acceleration sensor is subjected to a certain external acceleration in the *X* axis, the PTFE and Al electrodes, which are in the 1D acceleration sensor placed along *X* axis, can only render relative motion, while there are no relative motions between the PTFE and Al electrodes in the other 1D acceleration sensors placed along the *Y* and *Z* axes. Therefore, as shown in Figure 5a, the output voltage of the 3D acceleration sensor can characterize the acceleration in the *X* direction, and the output voltages for the *Y* and *Z* axes are zero, which is accord well with the structural design and working principle. The measurement range is +13.0 to +40.0 m/s^2 for the +*X* axis and −13.0 to −41.0 m/s^2 for the −*X* axis, which is not completely consistent due to the manufacturing and measuring error of the sensor. When the acceleration smaller than ±13 m/s^2 is applied to the sensor, owing to the friction between the PTFE and Al foil, the PTFE will not slide and the acceleration cannot be measured under the measurement lower limit. While when the sensor is subjected to the acceleration larger than +40.0 or −41.0 m/s^2, the sliding displacement will exceed 9 mm. In this state, all the positive charges on the electrode,

DOI: 10.1021/acsami.5b04516
ACS Appl. Mater. Interfaces XXXX, XXX, XXX−XXX

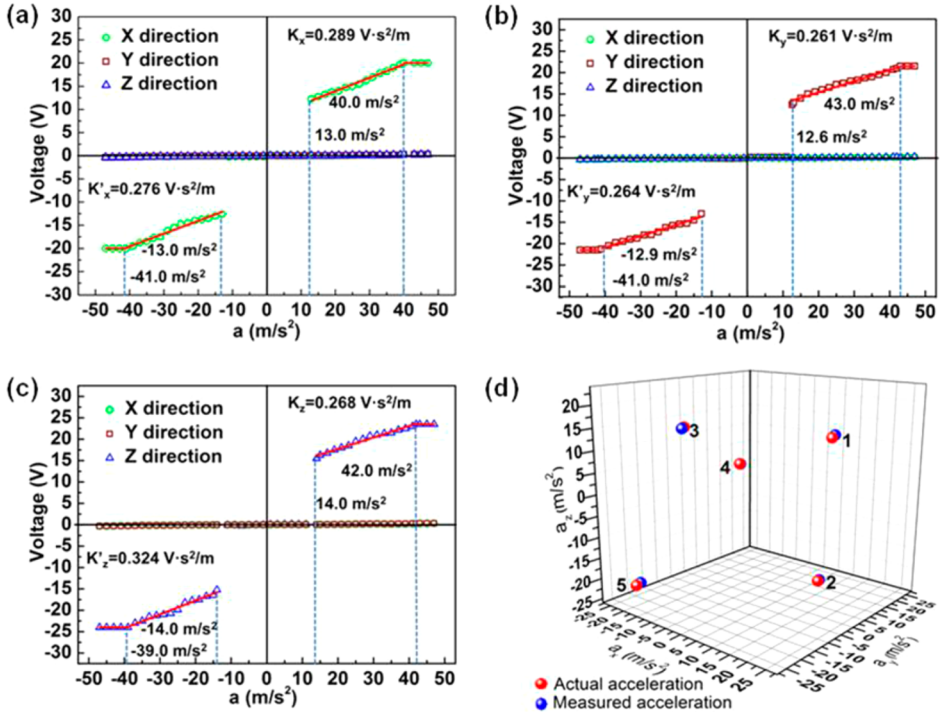

Figure 5. Characteristic calibrations of the 3D acceleration sensor in the three directions and the measurement results of the vector accelerations. (a–c) When the 3D acceleration sensor is subjected to a certain external acceleration in one axis, the 3D acceleration sensor can generate voltage to characterize acceleration in this axis, and there is no output voltage signal for the other two axes. (d) Measurement results of five vector accelerations. The measured vector accelerations accord closely with the actual accelerations.

which are completely separate with the PTFE film, will lose the constraints by the negative charges on the PTFE surface. Therefore, the potential difference of the two Al electrodes will not increase anymore and the acceleration sensor reaches the measurement upper limit. Figure 5b and c are the performances of the 3D acceleration sensor along the *Y* and *Z* axes, respectively. They have a similar performance with the one along the *X* axis. The detailed characteristics of the 3D acceleration sensor in three axes are listed in Table 1. The triple output voltages can characterize the components of the vector acceleration in the three axes, respectively and independently. Therefore, the 3D acceleration sensor can measure vector acceleration in any direction. By calculating the three output voltages, the vector acceleration can be obtained. As shown in Figure 5d, the red points represent the actual vector accelerations and the blue points represent the measured vector accelerations. It is obvious that the measured 3D vector accelerations accord closely with the actual accelerations. The measured components of the accelerations in the three axes have a maximum error of 0.9 m/s^2, which is within the standard deviation range. Therefore, the experimental results demonstrate that the sensor can correctly and effectively measure 3D vector accelerations in any directions. The detailed measurement data are shown in Table 2.

A collision experiment is simulated to demonstrate the application of the 3D acceleration sensor in the vehicle collision safety system. Figure 6a is a schematic illustration of the 3D acceleration sensor for practical application. When a vehicle collision accident took place, the impact acceleration can be measured and the safety air bag can be triggered by the acceleration sensor to protect human life. Generally, the time of the vehicle collision is very short and the impact acceleration is usually high, which is beyond the measurement upper limit of

Table 1. Detailed Characteristics of the 3D Acceleration Sensor in Three Axes

direction	a_{min} (m/s^2)	a_{max} (m/s^2)	S (V·s^2/m)[a]	R^2 [b]	SD (m/s^2)[c]
−*X*	−13.0	−41.0	0.276	0.977	1.349
+*X*	13.0	40.0	0.289	0.990	0.924
−*Y*	−12.9	−41.0	0.264	0.982	1.151
+*Y*	12.6	43.0	0.261	0.978	1.524
−*Z*	−14.0	−39.0	0.324	0.977	1.248
+*Z*	14.0	42.0	0.268	0.982	1.151

[a]*S* is the sensitivity of the sensor. [b]*R* is the coefficient to represent the correlation between the fitting curve and the experiment dates. [c]SD is the standard deviation.

Table 2. Detailed Measurement Results of the 3D Vector Accelerations

number	actual accelerations in three axis (m/s^2)			measured accelerations in three axis (m/s^2)			acceleration error (m/s^2)		
1	(12.1	12.1	12.1)	(12.7	12.6	12.8)	(0.6	0.5	0.7)
2	(17.7	0	−17.7)	(18.1	0	−17.3)	(0.4	0	−0.4)
3	(0	−25.4	17.8)	(0	−21.6	17.6)	(0	0.7	−0.2)
4	(25.0	−20.0	0)	(24.8	−20.1	0)	(−0.2	0.1	0)
5	(−22.0	−22.0	−22.0)	(−21.4	−21.1	−21.4)	(−0.6	−0.9	−0.6)

DOI: 10.1021/acsami.5b04516
ACS Appl. Mater. Interfaces XXXX, XXX, XXX−XXX

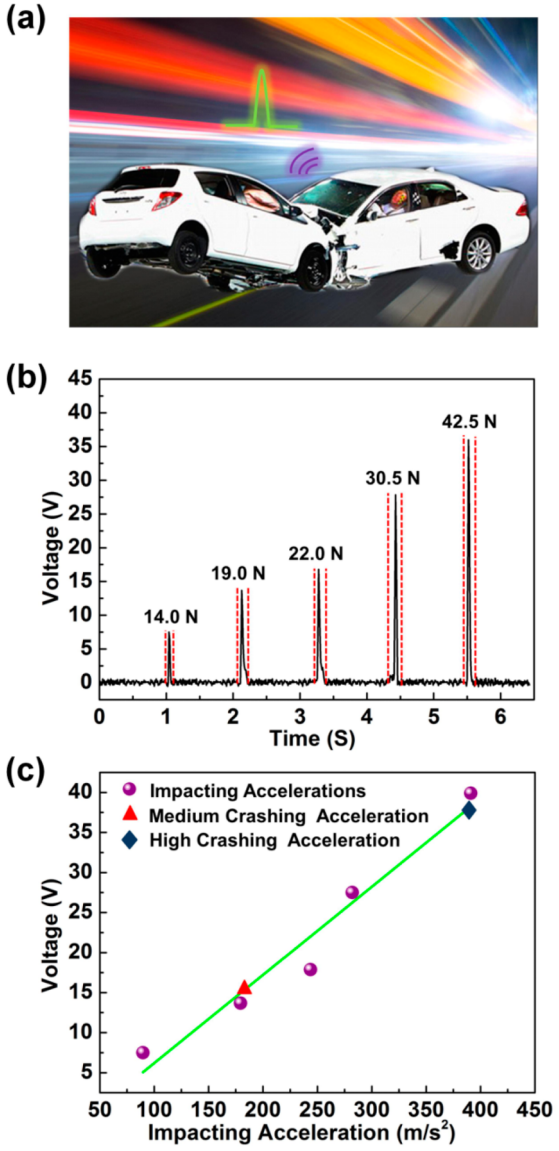

Figure 6. Application of the acceleration sensor in vehicle collision safety system. (a) Acceleration sensor for the application of the vehicle collision safety system. (b) Output voltages of the acceleration sensor in different impact forces. (c) Relationship between the output voltage and the impact acceleration. With the speed of 80 km/h, the car collision acceleration is about 180 m/s^2. When the car collision happened with a high speed of 120 km/h, the car collision acceleration can reach to about 400 m/s^2. The general and high car collision accelerations are in the measurement range of the acceleration sensor.

the designed acceleration sensor. In order to improve the measurement upper limit of the acceleration sensor, two springs with a spring coefficient of 103.84 N/m are used and the length of the PTFE film is increased to 35 mm. Owing to the limitation of the linear motor, which cannot apply a large acceleration to the sensor, a new experimental method was adopted to simulate the acceleration in vehicle collision. In this experiment, as shown in Figure S4 (Supporting Information), the sensor was fixed on the force gauge (MARK-10-M5-50) and impacted by the external collision force. By the measured values of the force gauge and the basic mechanical formula $F = Ma$, where M is the mass of the sensor system, the impacting accelerations can be calculated. Figure 6b shows the output voltages of the acceleration sensor with different collision forces. As shown in Figure 6c, the output voltage increases with the increasing of the impact acceleration. If two 1200 kg cars frontal collision happened, the maximum impact acceleration can reach about 180 and 400 m/s^2 corresponding to the running speed of 80 and 120 km/h,[31] which are in the measurement range of the 3D acceleration sensor. It indicates that the 3D acceleration sensor can measure high accelerations and has the potential application in the automobile security system.

CONCLUSION

In summary, we first developed a self-powered 3D acceleration sensor based on three independently and mutually perpendicular TENGs with an outer transparent shell and an inner mass-spring-damper mechanical system. The relationship between the output voltages and the sliding displacements of the PTFE film was systematically investigated. When an external acceleration in axis direction was applied to the TENG, the output voltage is generated and it had a good linear relationship with the external acceleration. Therefore, the TENG can be used as the acceleration sensor and it has good performance with the detection range from about 13.0 to 40.0 m/s^2 and sensitivity of 0.289 V·s^2/m in the axis direction. After 4000 cycles, the output voltages show only a little decay of ~6% and the acceleration sensor has an excellent stability. The three output voltages of the acceleration sensor can characterize the components of the vector acceleration in the three axes, respectively and independently. Therefore, the 3D acceleration sensor can measure vector acceleration in any direction. The measured components of the accelerations in the three axes have a maximum error of 0.9 m/s^2, which is within the standard deviation range. The 3D acceleration sensor can measure high collision accelerations and has the potential practicability in the automobile security system. This study not only demonstrates a self-powered and high sensitivity 3D acceleration sensor but also expands TENG's application in self-powered sensor fields.

EXPERIMENTAL SECTION

Fabrication of the Nanostructure on the Surface of the PTFE Film. The PTFE film (50 μm thick) was cleaned with isopropyl, alcohol and deionized water in sequence. It was blown dry with compressed air and deposited a layer of gold particles as the mask by sputtering. Subsequently, the PTFE film was processed by the inductively coupled plasma (ICP) for 40 s and the nanostructure was created on the surface. Specifically, Ar and O_2 gases were imported in the chamber with the flow of 5.0 and 55.0 sccm, respectively. One power source of 440 W was used to generate a large density of plasma and the other power source of 100 W was used to accelerate the plasma ions. The SEM image of the nanostructure was taken by Hitach S-5500.

Fabrication of the Acceleration Sensor. Twenty-four pieces of Al adhesive tape (50 μm thick) were cleaned and cut into rectangle (18 mm × 40 mm). Then they were pasted on 12 pieces of acrylic sheets, respectively. The PTFE film, sponge and mass's surface were pasted in sequence. Finally, the mass and springs were sealed in the acrylic sheet shell.

ASSOCIATED CONTENT

Supporting Information

The Supporting Information is available free of charge on the ACS Publications website at DOI: 10.1021/acsami.5b04516.

Additional schematic figures illustrating the relationship between the sliding displacement and the output voltage, charge distribution in the friction surfaces, the relation-

DOI: 10.1021/acsami.5b04516
ACS Appl. Mater. Interfaces XXXX, XXX, XXX−XXX

ship between the peak value of output voltage, the corresponding acceleration along the −*X* direction, and the experimental method of high accelerations (PDF)

AUTHOR INFORMATION

Corresponding Authors

*E-mail: zlwang@gatech.edu (Z.L.W.)
*E-mail: czhang@binn.cas.cn (C.Z.).

Notes

The authors declare no competing financial interest.

ACKNOWLEDGMENTS

The project is supported by National Natural Science Foundation of China (Grant No. 51475099, Grant No. 51432005), the "thousands talents" program for the pioneer researcher, and the Youth Innovation Promotion Association, CAS. We also thank Libo Chen for the discussions.

REFERENCES

(1) Roylance, L. M. A Miniature Integrated Circuit Accelerometer for Biomedical Application. Ph. D. dissertation, Department of Electrical Engineering, Stanford University, Stanford, CA,1977.

(2) Zimmermann, L.; Ebersohl, J.; Hung, F.; Berry, J. P.; Baillieu, F.; Rey, P.; Diem, B.; Renard, S.; Caillat, P. Airbag Application: A Microsystem Including a Silicon Capacitive Accelerometer, CMOS Switched Capacitor Electronics and True Self-test Capability. *Sens. Actuators, A* **1995**, *46*, 190−195.

(3) Li, G.; Li, Z. H.; Wang, C. S.; Hao, Y. L.; Li, T.; Zhang, D. C.; Wu, G. Y. Design and Fabrication of a Highly Symmetrical Capacitive Triaxial Accelerometer. *J. Micromech. Microeng.* **2001**, *11*, 48−54.

(4) Liu, S. F.; Ma, T. H.; Hou, W. Design and Fabrication of a New Miniaturized Capacitive Accelerometer. *Sens. Actuators, A* **2008**, *147*, 70−74.

(5) Chen, H.; Shen, S. Q.; Bao, M. H. Over-range Capacity of a Piezoresistive Microaccelerometer. *Sens. Actuators, A* **1997**, *58*, 197−201.

(6) Nemirovsky, Y.; Nemirovesky, A.; Muralt, P.; Setter, N. Design of a Novel Thin-film Piezoelectric Accelerometer. *Sens. Actuators, A* **1996**, *56*, 239−249.

(7) Hindrichsen, C. C.; Almind, N. S.; Brodersen, S. H.; Lou-Moller, R.; Hansen, K.; Thomsen, E. V. Triaxial MEMS Accelerometer with Screen Printed PZT Thick Film. *J. Electroceram.* **2010**, *25*, 108−115.

(8) Scheeper, P.; Gullov, J. O.; Kofoed, L. M. A Piezoelectric Triaxial Accelerometer. *J. Micromech. Microeng.* **1996**, *6*, 131−133.

(9) Yang, Y.; Zhang, H. L.; Zhu, G.; Lee, S.; Lin, Z. H.; Wang, Z. L. Flexible Hybrid Energy Cell for Simultaneously Harvesting Thermal, Mechanical, and Solar Energies. *ACS Nano* **2013**, *7*, 785−790.

(10) O'Regan, B.; Gratzel, M. A Low-cost, High-efficiency Solar Cell Based on Dye-sensitized Colloidal TiO_2 Films. *Nature* **1991**, *353*, 737−740.

(11) Xie, Y. N.; Wang, S. H.; Lin, L.; Jing, Q. S.; Lin, Z. H.; Wang, Z. L.; Niu, Z.; Wang, Z. Rotary Triboelectric Nanogenerator Based on a Hybridized Mechanism for Harvesting Wind Energy. *ACS Nano* **2013**, *7*, 7119−7125.

(12) Wu, Y. C.; Zhong, X. D.; Wang, X.; Yang, Y.; Wang, Z. L. Hybrid Energy Cell for Simultaneously Harvesting Wind, Solar, and Chemical Energies. *Nano Res.* **2014**, *7*, 1631−1639.

(13) Zhang, H.; Yang, Y.; Su, Y.; Chen, J. J.; Adams, K.; Lee, S.; Hu, C. G.; Wang, Z. L. Triboelectric Nanogenerator for Harvesting Vibration Energy in Full Space and as Self-Powered Acceleration Sensor. *Adv. Funct. Mater.* **2014**, *24*, 1401−1407.

(14) Wang, Z. L. Triboelectric Nanogenerators as New Energy Technology for Self-powered Systems and as Active Mechanical and Chemical Sensors. *ACS Nano* **2013**, *7*, 9533−9557.

(15) Fan, F. R.; Tian, Z. Q.; Wang, Z. L. Flexible Triboelectric Generator. *Nano Energy* **2012**, *1*, 328−334.

(16) Zhang, C.; Tang, W.; Han, C. B.; Fan, F. R.; Wang, Z. L. Theoretical Comparison, Equivalent Transformation, and Conjunction Operations of Electromagnetic Induction Generator and Triboelectric Nanogenerator for Harvesting Mechanical Energy. *Adv. Mater.* **2014**, *26*, 3580−359.

(17) Tang, W.; Han, C. B.; Zhang, C.; Wang, Z. L. Cover-sheet-based Nanogenerator for Charging Mobile Electronics Using Low-frequency Body Motion/Vibration. *Nano Energy* **2014**, *9*, 121−127.

(18) Han, C. B.; Zhang, C.; Tang, W.; Li, X. H.; Wang, Z. L. High Power Triboelectric Nanogenerator Based on Printed Circuit Board (PCB) Technology. *Nano Res.* **2015**, *8*, 722−730.

(19) Zhang, C.; Tang, W.; Zhang, L. M.; Han, C. B.; Wang, Z. L. Contact Electrification Field-Effect Transistor. *ACS Nano* **2014**, *8*, 8702−8709.

(20) Zhang, C.; Tang, W.; Pang, Y. K.; Han, C. B.; Wang, Z. L. Active Micro-actuators for Optical Modulation Based on a Planar Sliding Triboelectric Nanogenerator. *Adv. Mater.* **2015**, *27*, 719−726.

(21) Chen, M. X.; Li, X. Y.; Lin, L.; Du, W. M.; Han, X.; Zhu, J.; Pan, C. F.; Wang, Z. L. Triboelectric Nanogenerators as a Self-powered Motion Tracking System. *Adv. Funct. Mater.* **2014**, *24*, 5059−5066.

(22) Fan, F. R.; Lin, L.; Zhu, G.; Wu, W. Z.; Zhang, R.; Wang, Z. L. Transparent Triboelectric Nanogenerators and Self-powered Pressure Sensors Based on Micropatterned Plastic Films. *Nano Lett.* **2012**, *12*, 3109−3114.

(23) Zhu, G.; Yang, W. Q.; Zhang, T.; Jing, Q.; Chen, J.; Zhou, Y. S.; Bai, P.; Wang, Z. L. Self-powered, Ultrasensitive, Flexible Tactile Sensors Based on Contact Electrification. *Nano Lett.* **2014**, *14*, 3208−3214.

(24) Lin, L.; Xie, Y. N.; Wang, S. H.; Wu, W. Z.; Niu, S. M.; Wen, X. N.; Wang, Z. L. Triboelectric Active Sensor Array for Self-powered Static and Dynamic Pressure Detection and Tactile Imaging. *ACS Nano* **2013**, *7*, 8266−8274.

(25) Yang, Y.; Zhang, H. L.; Lin, Z. H.; Zhou, Y. S.; Jing, Q. S.; Su, Y. J.; Yang, J.; Chen, J.; Hu, C. G.; Wang, Z. L. Human Skin Based Triboelectric Nanogenerators for Harvesting Biomechanical Energy and as Self-powered Active Tactile Sensor System. *ACS Nano* **2013**, *7*, 9213−9222.

(26) Yu, A. F.; Song, M.; Zhang, Y.; Zhang, Y.; Chen, L. B.; Zhai, J. Y.; Wang, Z. L. Self-powered Acoustic Source Locator in Underwater Environment Based on Organic Film Triboelectrific Nanogenerator. *Nano Res.* **2015**, *8*, 765−773.

(27) Yang, J.; Chen, J.; Liu, Y.; Yang, W. Q.; Su, Y. J.; Wang, Z. L. Triboelectrification-based Organic Film Nanogenerator for Acoustic Energy Harvesting and Self-powered Active Acoustic Sensing. *ACS Nano* **2014**, *8*, 2649−2657.

(28) Hu, Y. F.; Yang, J.; Jing, Q. S.; Niu, S. M.; Wu, W. Z.; Wang, Z. L. Triboelectric Nanogenerator Built on Suspended 3D Spiral Structure as Vibration and Positioning Sensor and Wave Energy Harvester. *ACS Nano* **2013**, *7*, 10424−10432.

(29) Wang, S. H.; Niu, S. M.; Yang, J.; Lin, L.; Wang, Z. L. Quantitative Measurements of Vibration Amplitude Using a Contact-Mode Freestanding Triboelectric Nanogenerator. *ACS Nano* **2014**, *8*, 12004−12013.

(30) Chen, J.; Zhu, G.; Yang, W.; Jing, Q.; Bai, P.; Yang, Y.; Hou, T. C.; Wang, Z. L. Harmonic-resonator-based Triboelectric Nanogenerator as a Sustainable Power Source and a Self-powered Active Vibration Sensor. *Adv. Mater.* **2013**, *25*, 6094−6099.

(31) Wagstrom, L.; Thomson, R.; Pipkorn, B. Structural Adaptivity for Acceleration Level Reduction in Passenger Car Frontal Collisions. *Int. J. Crashworthiness* **2004**, *9*, 121−127.

DOI: 10.1021/acsami.5b04516
ACS Appl. Mater. Interfaces XXXX, XXX, XXX−XXX